J Mater Sci (2011) 46:5129–5139
DOI 10.1007/s10853-011-5444-5

Effect of process parameters on size, shape, and distribution of Sb_2O_3 nanoparticles

Hui Shun Chin · Kuan Yew Cheong · Khairunisak Abdul Razak

Received: 1 December 2010 / Accepted: 5 March 2011 / Published online: 18 March 2011

Abstract Antimony trioxide (Sb_2O_3) nanoparticles with particle sizes ranging from 2 to 12 nm, spherical in shape, and well-distributed were successfully synthesized by chemical reduction method. The nanoparticles were synthesized in the presence of hydrazine as a reduction agent in ethylene glycol through the reaction between antimony trichloride and sodium hydroxide. Effects of reaction temperature, reaction time, precursor concentration and boiling temperature on the particle size, shape, and distribution of the Sb_2O_3 nanoparticles were investigated. Morphology of the nanoparticles was examined by transmission electron microscope (TEM). It was revealed that the particle size increased when reaction temperature, reaction time and concentration of precursor were increased. Moreover, the mixture needed to be boiled prior to the addition of hydrazine as a reduction agent, in order to obtain an optimum reduction. X-ray diffraction (XRD) was employed to study the crystallinity and phase of the nanoparticles. The nanoparticles were determined as cubic phase of Sb_2O_3 (ICDD file no. 00-043-1071) by XRD. Interrelation between UV–vis absorption spectra of the nanoparticles and their particle size were obtained.

Introduction

At present time, progressive development of nanotechnology has triggered the synthesis of particles in nanometer scale. Nanoparticles possess novel electronic, chemical, mechanical, optical, sensing and catalytic properties, which are different from those bulk materials due to their high surface-to-volume ratio [1, 2]. These properties find applications in the field of flame retardant synergist, catalyst, optical material, sensor, electronic and optoelectronic devices [3–10]. Nanoparticles are commonly incorporated in polymers acting as a flame retardant compound to prevent burning of the polymers. There are some commonly used flame retardants such as antimony trioxide (Sb_2O_3), aluminum trihydrate, and magnesium hydroxide [4]. Among those reported candidates, Sb_2O_3 is a well known flame retardant synergist, which is applied in plastics and rubber. However, larger particle size and lower mechanical properties of Sb_2O_3 particles have limited their applications [4]. Thus, most efforts have been focused to synthesize Sb_2O_3 nanoparticles in the smallest size, with spherical shape and well distribution.

Up to now, Sb_2O_3 nanoparticles have been successfully synthesized in polyhedral shape with particle size less than 200 nm by chemical method [11]. This method enables Sb_2O_3 to be synthesized in nanoparticles form at the shortest time ($\sim$1 h) with the lowest cost and simplest route, if compared to other reported methods [12–19]. In this method, polyvinyl alcohol (PVA) and sodium hydroxide (NaOH) were used to synthesize the Sb_2O_3 nanoparticles. However, larger particle size with polyhedral shape has limitation in their application as flame retardant synergist. To overcome this issue, the chemical method had been modified into chemical reduction method, where hydrazine (N_2H_5OH) acting as a reducing agent and ethylene glycol (EG) acting as a protective agent solvent were introduced. It was reported that this chemical reducing method was able to synthesize nanoparticles of nickel (Ni) with mean particle size of 9.2 nm in spherical shape

H. S. Chin · K. Y. Cheong (✉) · K. Abdul Razak
Energy Efficient & Sustainable Semiconductor Research Group, School of Materials and Mineral Resources Engineering, Universiti Sains Malaysia, 14300 Nibong Tebal, Penang, Malaysia
e-mail: cheong@eng.usm.my

and the size was distributed uniformly [20]. In the system of cobalt (Co), particle size ranging from 4 to 13 nm in spherical shape with well distribution were successfully synthesized by reduction of Co^{2+} with hydrazine in EG [21].

In chemical reduction method, there are a few process parameters that contribute to the particle size, shape, and size distribution of nanoparticles. Some of the reported parameters are concentration of hydrazine, NaOH and precursor, reaction temperature, and reaction time [21–28]. Increasing reaction temperature [26, 27], reaction time [22, 23, 25], and concentration of precursor [21, 24] exhibited greater effect on the growth rather than on the nucleation of other systems, where particle size increased with the increase of reaction temperature, reaction time, and concentration of precursor, respectively. The effect of hydrazine and NaOH concentration on Sb_2O_3 nanoparticles had been reported via chemical reducing method [28]. It was found that the particle size decreased and remained constant (2–12 nm) when $[N_2H_5OH]/[Sb^{3+}] \geq 10$ and $[NaOH]/[Sb^{3+}] = 3$. In order to further improve the particle size, shape, and size distribution of Sb_2O_3 nanoparticles, the aforementioned three effects (concentrations of precursor, reaction temperature, and reaction time) and boiling temperature have been investigated in this study.

Experimental

The synthesis of Sb_2O_3 nanoparticles was carried out in a fume cupboard. The precursor was prepared by dissolving 25 mM of $SbCl_3$ in EG. Subsequently, an appropriate amount of NaOH ($[NaOH]/[Sb^{3+}] = 3$) was added to the above solution under a constant stirring. The mixture was heated until it boiled, immediately after that, an appropriate amount of hydrazine ($[N_2H_5OH]/[Sb^{3+}] = 10$) was added into the mixture under vigorous stirring condition. The mixture was stirred for 60 min at various reaction temperatures (60, 90, 120, and 150 °C) until white precipitates were obtained. Then, the precipitates were filtered by washing several times with distilled water and ethanol. After that, the precipitates were dried at 100 °C for 1 h. Same procedures were repeated under different parameters when the effect of reaction time (30, 60, 90, and 120 min), concentration of precursor ($[Sb^{3+}]/[N_2H_5OH] = 0.05$, 0.1, 0.15, and 0.2), and boiling temperature (25, 50, 80, and 110 °C) were investigated.

The particle size was examined by using a CM Philips transmission electron microscope (TEM) operated at 120 kV. For one sample, a total of 300 particles were measured to determine the particles size, as well as their size distribution. This analysis was carried out by ImageJ software. Crystalline phases of nanoparticles were detected by a D500 Siemens diffractometer using Cu-Kα_1 radiation with $\lambda = 1.5406$ Å as an X-ray source and was adjusted at a voltage of 40 kV and a current of 40 mA. X-ray diffraction (XRD) measurements were scanned from $2\theta = 10°$–$90°$ by using a step time of 71.60 s and step size of 0.034°. A Perkin Elmer spectrophotometer equipped with a 10 mm quartz cell was employed to obtain UV–vis absorption spectra of the nanoparticles.

Results and discussions

Effect of reaction temperature

In order to study the effect of reaction temperature on the particle size, shape, and size distribution of the nanoparticles, other process parameters were fixed. Those fixed process parameters were concentration of hydrazine at $[N_2H_5OH]/[Sb^{3+}] = 10$, concentration of NaOH at $[NaOH]/[Sb^{3+}] = 3$, reaction time at 60 min, concentration of precursor at $[Sb^{3+}]/[N_2H_5OH] = 0.1$, and boiling temperature at 110 °C.

Figure 1 shows TEM images and histogram of particle size distribution of as-synthesized nanoparticles prepared at different reaction temperatures (60, 90, 120, and 150 °C). At 60 °C (Fig. 1a), no nanoparticles were observed, but some fibrous materials were formed after heating for 60 min. It may be due to slow reduction rate of Sb^{3+} by hydrazine. Since no nanoparticles were formed at 60 °C, the reaction temperature was then increased to 90 °C. At this temperature, mixture of fibrous materials and nanoparticles were found as presented in Fig. 1b. Formation of the mixture was due to incomplete reduction of Sb^{3+}, where those un-reduced Sb^{3+} were tended to form fibrous materials and those reduced Sb^{3+} were underwent nucleation and oxidization processes to form oxide nanoparticles. As the reaction temperature was increased to 120 °C, nanoparticles with well-distributed spherical shape (Fig. 1c) were observed and the particle size is ranged from 2 to 12 nm (Fig. 1e). These promising findings offer a viable solution to the issue raised by Zhang et al. [11], in which their Sb_2O_3 particles were in polyhedral shape with particle size less than 200 nm that will limit their applications.

The formation mechanism of Sb_2O_3 nanoparticles can be explained by four processes [28], i.e., reduction, nucleation, oxidization, and growth. At first, ion Sb^{3+} is reduced to Sb atom by hydrazine as shown in Eq. 1

$$4Sb^{3+} + 3N_2H_4 + 12OH^- \rightarrow 4Sb + 3N_2 + 12H_2O. \quad (1)$$

Nucleation occurs to form nuclei by collision between formed Sb atoms. Subsequently, growth process is initiated once the nuclei are formed. Sb_2O_3 nanoparticles are formed

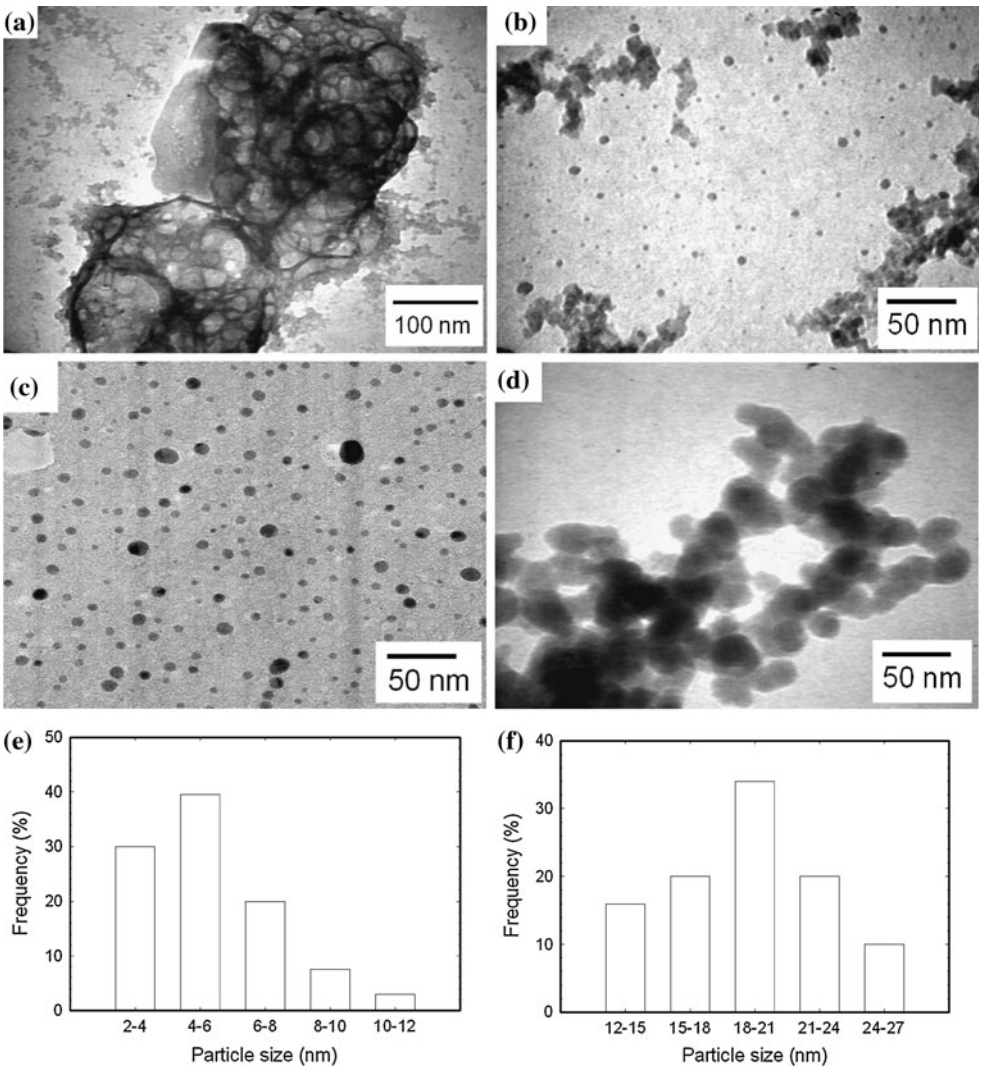

Fig. 1 TEM images of Sb_2O_3 nanoparticles with effect of reaction temperature **a** 60 °C, **b** 90 °C, **c** 120 °C [28] (With kind permission from Springer Science+Business Media: Journal of Nanoparticle Research, Controlled synthesis of Sb_2O_3 nanoparticles by chemical reducing method in ethylene glycol, DOI 10.1007/s11051-010-0169-y, 2010, Hui Shun Chin, Kuan Yew Cheong, Khairunisak Abdul Razak, Fig. 1c), and **d** 150 °C and the corresponding particle size distribution **e** 120 °C [28] and **f** 150 °C

when those grown nuclei are oxidized in environment, as shown in Eq. 2

$$4Sb + 3O_2 \rightarrow 2Sb_2O_3. \quad (2)$$

Since both oxidization and growth process happen simultaneously, there is a possibility to form a core–shell structure of Sb–Sb_2O_3. The core–shell structure may form if the growth rate is faster than oxidization rate. In this study, based on TEM images, none of any structures with dark core capping with lighter shell were observed, thus, core–shell structure of Sb_2O_3 nanoparticles did not form. It is suggested that the oxidization rate is faster than the growth rate. Meanwhile, the presence of well-distributed nanoparticles may be due to extremely fast nucleation rate, which attributes to a complete separation of nucleation and the growth process.

By further increasing of the reaction temperature to 150 °C, nanoparticles with spherical shape were nearly agglomerated as shown in Fig. 1d. The agglomeration may be due to ripening effect [26], where larger particles are formed from those smaller particles, which have higher surface energy than the larger ones. Besides, Rautio et al. [29] reported that at higher temperature, polymeric network of nanoparticles collapsed and nanoparticles were able to grow easily. Figure 1e and f presents particle size distribution of Sb_2O_3 nanoparticles. It is clearly seen that the particle size distribution became broader from 2–12 nm to 12–27 nm, when reaction temperature was increased from 120 to 150 °C, respectively. It is also noted that the predominated size range was increased from 4–6 nm (mean particle size: 4.72 nm) to 18–21 nm (mean particle size: 18.97 nm), as the reaction temperature was increased from 120 to 150 °C. Similar trend had been reported by other researchers [26, 27]. However, mean particle size of Sb_2O_3 nanoparticles prepared at 60 °C and 90 °C could not be measured because no nanoparticles were formed at 60 °C and mixture of fibrous materials and nanoparticles were formed at 90 °C.

The corresponding XRD patterns of Sb_2O_3 nanoparticles at different reaction temperatures are shown in Fig. 2. A mixture of amorphous and polycrystalline phases were detected in sample prepared at 60 °C (Fig. 2a). Those phases were stable unless altering them with heat treatment. The amorphous phase was detected at diffraction angle $2\theta < 27°$. Similar findings were found at 90 °C (Fig. 2b), where both amorphous and polycrystalline phases were detected. But, the amorphous phase ($2\theta < 27°$) gradually decreased while the crystalline phase gradually appeared, as denoted by the appearance of diffraction peaks at $2\theta > 60°$. At 120 °C, all of the diffraction peaks matched with cubic phase of Sb_2O_3 (ICDD file no. 00-043-1071) as shown in Fig. 2c. Those matched diffraction peaks were associated with (222), (400), (331), (440), (622), (444), (551), (731), (800), (733), (662), (840) and (844) planes. They are in good agreement with the findings reported by Zhang et al. [11] and Zeng et al. [16]. From the XRD pattern, no other impurities were detected. As reaction temperature was increased to 150 °C (Fig. 2d), same diffraction peaks were detected at reaction temperature of 120 °C. However, intensities of those peaks were of higher intensity and sharper as compared to reaction temperature at 120 °C. This is associated with the increase in the Sb_2O_3 nanoparticles size.

Figure 3 depicts typical UV–vis absorption spectra of Sb_2O_3 nanoparticles obtained from different reaction temperatures (60, 90, 120, and 150 °C). Overall, the maximum absorption wavelengths occurred at the range of 280–314 nm, which are consistent with the literature, where the maximum absorption wavelength occurred at the range of 200–360 nm [15] and 250–300 nm [30]. The maximum absorption wavelengths of reaction temperature at 120 °C and 150 °C were 280 nm and 298 nm, respectively. The shifting of maximum absorption wavelength to

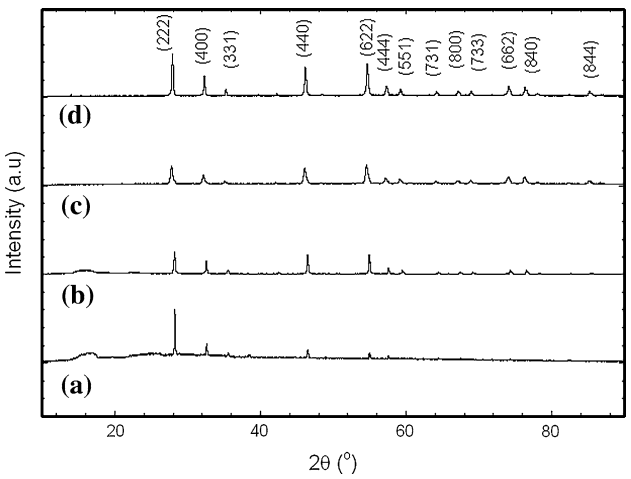

Fig. 2 XRD patterns of Sb_2O_3 nanoparticles with effect of reaction temperature (*a*) 60 °C, (*b*) 90 °C, (*c*) 120 °C [28], and (*d*) 150 °C

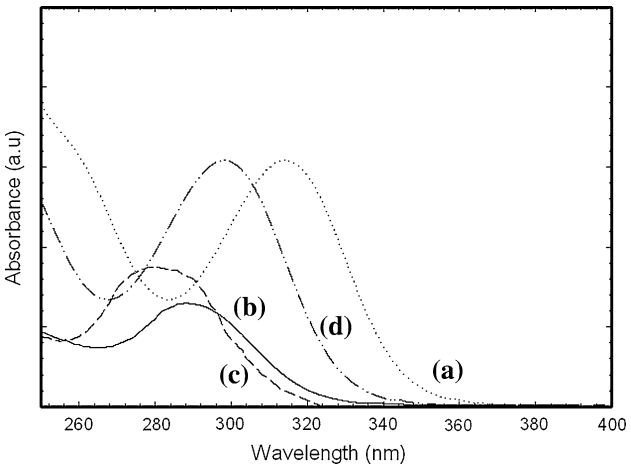

Fig. 3 UV–vis absorption spectra of Sb_2O_3 nanoparticles with effect of reaction temperature (*a*) 60 °C, (*b*) 90 °C, (*c*) 120 °C [28], and (*d*) 150 °C

a lower wavelength was due to the smaller particles formed at 120 °C nm (mean particle size: 4.72 nm) (Fig. 1c) as compared to particles formed at 150 °C (mean particle size: 18.97 nm) (Fig. 1d). At 90 °C, the maximum absorption wavelength was at 288 nm, between the maximum absorption wavelength of 120 °C (280 nm) and 150 °C (298 nm). This may be due to the mixture of both amorphous and crystalline phases that had been formed (Fig. 1b). The significant red-shift [26] of maximum absorption wavelength to 314 nm was detected at 60 °C, which may be attributed to the formation of larger fibrous materials (Fig. 1a).

Effect of reaction time

To understand the effect of reaction time on the particle size, shape, and size distribution of the nanoparticles, other process parameters are kept stable. Those process parameters were concentration of hydrazine at $[N_2H_5OH]/[Sb^{3+}] = 10$, concentration of NaOH at $[NaOH]/[Sb^{3+}] = 3$, reaction temperature at 120 °C, concentration of precursor at $[Sb^{3+}]/[N_2H_5OH] = 0.1$, and boiling temperature at 110 °C.

Transmission electron microscope (TEM) images and particle size distribution of Sb_2O_3 nanoparticles prepared at different reaction times (30, 60, 90, and 120 min) are presented in Fig. 4. At reaction time of 30 min (Fig. 4a), well-agglomerated particles were observed and the particle size distribution hardly measured. Therefore, this result was unable to be presented. Since there were no well-distributed nanoparticles, reaction time was increased to 60 min and well-distributed Sb_2O_3 nanoparticles with spherical shape were observed, as shown in Fig. 4b. Up to now, Sb_2O_3 nanoparticles with mean particle size of 4.72 nm, spherical in shape, and narrow particle size

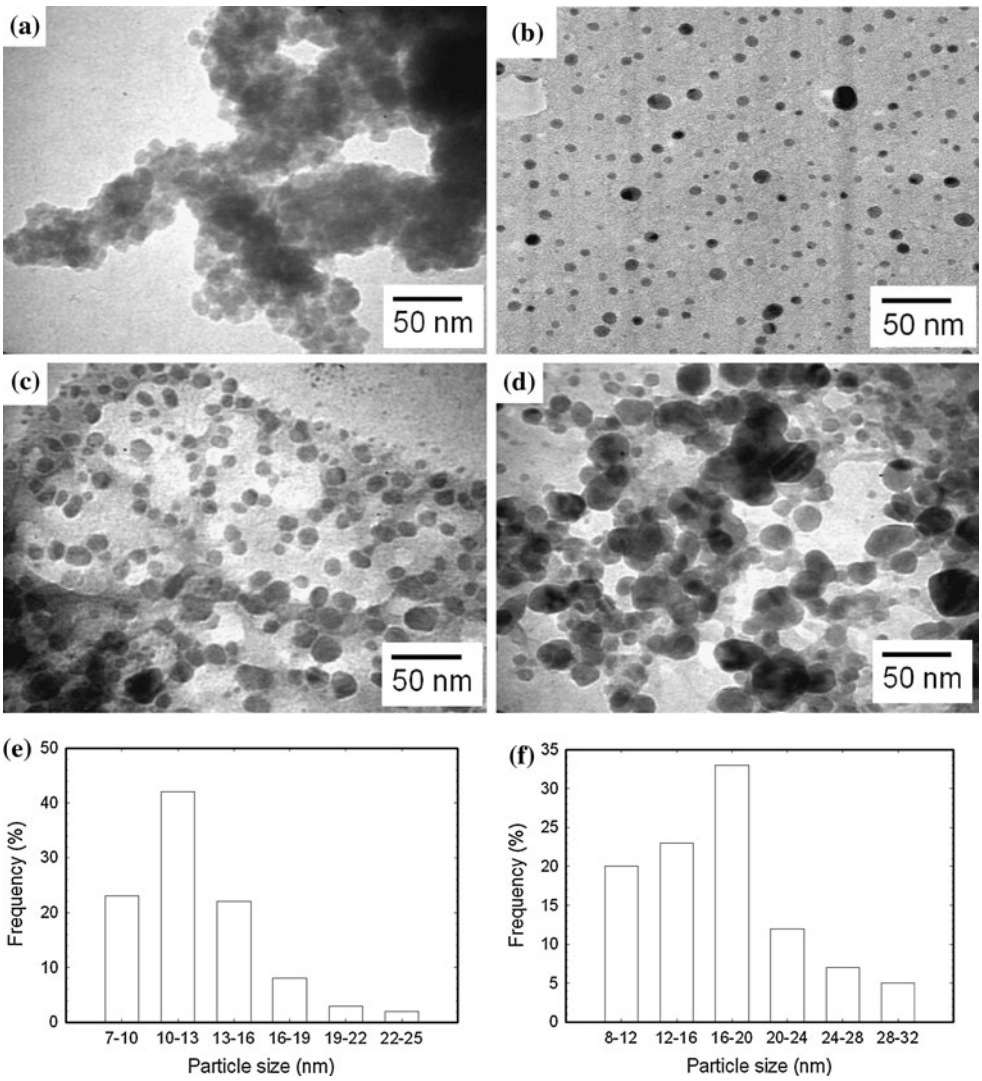

Fig. 4 TEM images of Sb_2O_3 nanoparticles with effect of reaction time **a** 30 min, **b** 60 min [28] (With kind permission from Springer Science+Business Media: Journal of Nanoparticle Research, Controlled synthesis of Sb_2O_3 nanoparticles by chemical reducing method in ethylene glycol, DOI 10.1007/s11051-010-0169-y, 2010, Hui Shun Chin, Kuan Yew Cheong, Khairunisak Abdul Razak, Fig. 1c), **c** 90 min, and **d** 120 min and the corresponding particle size distribution **e** 90 min and **f** 120 min

distribution (2–12 nm) is a promising finding as compared to other reported findings (less than 200 nm with polyhedral shape [11] and longer synthesizing time [2, 12, 13, 17]). As reaction time increased to 90 min and 120 min, the nanoparticles grew larger and nearly agglomerated, as presented in Fig. 4c and d. Particle size distribution became broader from 2–12 nm to 7–25 nm (mean particle size: 12.94 nm) (Fig. 4e) and 8–32 nm (mean particle size: 17.02 nm) (Fig. 4f), with respective to reaction time of 60 min, 90 min and 120 min in sequence. This occurrence was mainly due to the prolonged reaction time that accelerated growth rate of the nanoparticles gradually after oxidization process was completed. Thus, particle size of Sb_2O_3 nanoparticles increased when reaction time was increased from 60 to 120 min, as elucidated in Fig. 5. This trend had also been reported by Kim et al. [23] and Yang et al. [25].

Figure 6 shows XRD patterns of Sb_2O_3 nanoparticles at different reaction times. Mixture of amorphous and

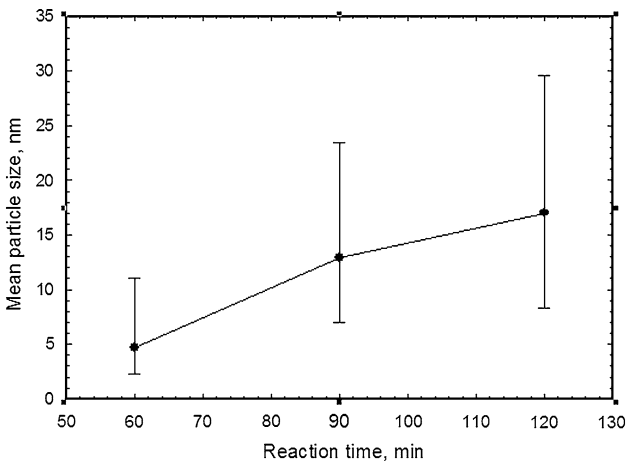

Fig. 5 Effect of reaction time on particle size of Sb_2O_3 nanoparticles. The *error bars* indicate the maximum, minimum, and mean values of the particle size. (Particle size at reaction time of 30 min could not measure because no particles were observed)

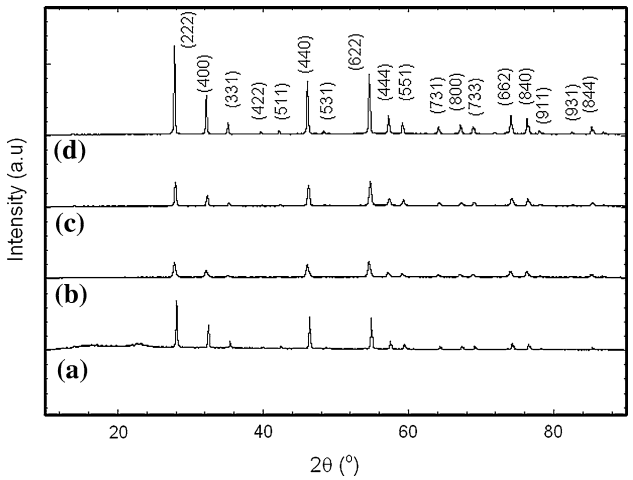

Fig. 6 XRD patterns of Sb_2O_3 nanoparticles with effect of reaction time (*a*) 30 min, (*b*) 60 min [28], (*c*) 90 min, and (*d*) 120 min

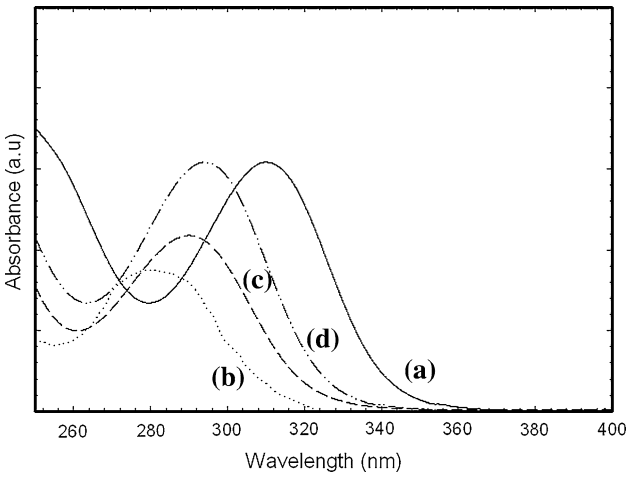

Fig. 7 UV–vis absorption spectra of Sb_2O_3 nanoparticles with effect of reaction time (*a*) 30 min, (*b*) 60 min [28], (*c*) 90 min, and (*d*) 120 min

polycrystalline phases in sample with reaction time of 30 min is shown in Fig. 6a. Amorphous phase was detected at $2\theta < 27°$ and some polycrystalline peaks were detected, which are in good agreement with cubic phase of Sb_2O_3 (ICDD file no. 00-043-1071). As reaction time increased to 60 min (Fig. 6b), the amorphous phase disappeared, but there were total of 13 diffraction peaks that had been detected. The detected diffraction peaks are associated with (222), (400), (331), (440), (622), (444), (551), (731), (800), (733), (662), (840) and (844) planes. All of the diffraction peaks can be indexed to cubic phase of Sb_2O_3 (ICDD file no. 00-043-1071). When reaction time increased to 90 min, similar diffraction peaks were detected as aforementioned, but the diffraction peaks became sharper with higher intensity when compared with reaction time at 60 min, as shown in Fig. 6c. It was due to the formation of larger Sb_2O_3 nanoparticles. By further increasing the reaction time to 120 min (Fig. 6d), same diffraction peaks were detected as compared to reaction time of 60 min and 90 min. However, additional five diffraction peaks were also detected, which are associated with (422), (511), (531), (911), and (931) planes. Nevertheless, the additional peaks also matched with the same ICDD file as discussed above. Moreover, those diffraction peaks exhibited the sharpest and highest intensity among other reaction times (60 and 90 min). The diffraction peaks with the sharpest and highest intensity are corresponded to the formation largest particles. Those detected diffraction peaks (60 min, 90 min and 120 min) were in agreement with the findings reported by Zhang et al. [11] and Zeng et al. [16]. From the XRD patterns (Fig. 6), it was also noted that cubic phase of Sb_2O_3 was the only phase detected and no other impurities.

UV–vis absorption spectra of Sb_2O_3 nanoparticles produced by different reaction times (30, 60, 90, and 120 min) are presented in Fig. 7. It is clearly seen that the maximum absorption wavelength took place from 280 to 310 nm, which are comparable with the previous reported findings (maximum absorption wavelength are occurred from 200 to 360 nm [15] and 250 to 300 nm [30]). At reaction time of 30 min, maximum absorption wavelength was occurred at 310 nm. When reaction time increased to 60, 90, and 120 min, the corresponding maximum absorption wavelengths were 280 nm (mean particle size: 4.72 nm), 290 nm (mean particle size: 12.94 nm), and 294 nm (mean particle size: 17.02 nm), respectively. Relative to the reaction time at 30 min, the maximum absorption wavelengths of reaction time at 60, 90, and 120 min were blue-shifted. It is well known that optical absorption would change accordingly to the changes of morphology and crystallinity of nanoparticles [25]. The shifting of the maximum absorption wavelength could be proved by varying the particle size of Sb_2O_3, as shown in Figs. 4 and 5, in which a blue-shift of maximum absorption wavelength was detected when the particle size decreased when the reaction time was decreased.

Effect of precursor concentration

Aiming to investigate the effect of concentration of precursor ($SbCl_3$) on the particle size, shape, and size distribution of the nanoparticles, other process parameters are kept constant. The constant process parameters were concentration of hydrazine at $[N_2H_5OH]/[Sb^{3+}] = 10$, concentration of NaOH at $[NaOH]/[Sb^{3+}] = 3$, reaction temperature at 120 °C, reaction time at 60 min and boiling temperature at 110 °C.

Figure 8 shows TEM images and particle size distribution of Sb_2O_3 nanoparticles with different concentrations of precursor ($[Sb^{3+}]/[N_2H_5OH] = 0.05$, 0.1, 0.15, and 0.2).

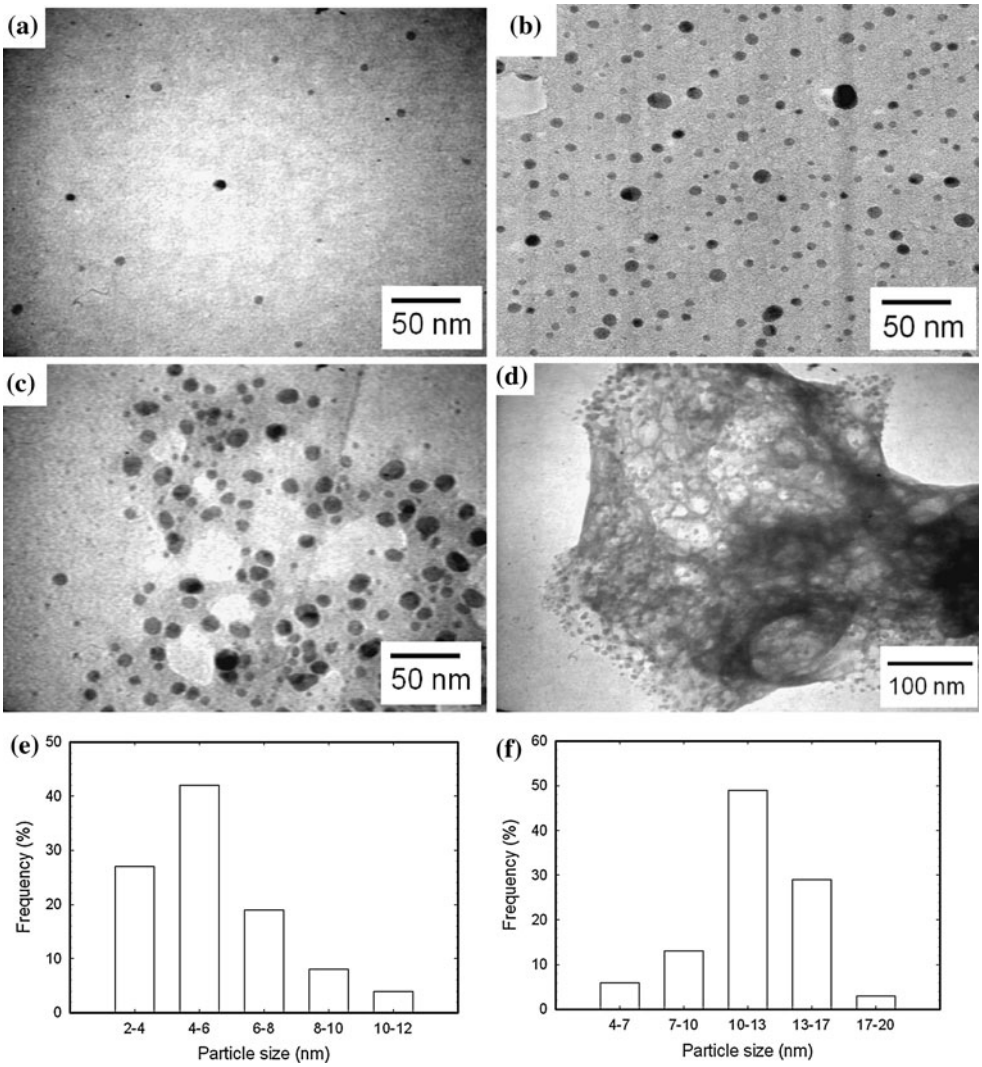

Fig. 8 TEM images of Sb_2O_3 nanoparticles with effect of concentration of precursor $[Sb^{3+}]/[N_2H_5OH]$ = **a** 0.05, **b** 0.1 [28] (With kind permission from Springer Science+Business Media: Journal of Nanoparticle Research, Controlled synthesis of Sb_2O_3 nanoparticles by chemical reducing method in ethylene glycol, DOI 10.1007/s11051-010-0169-y, 2010, Hui Shun Chin, Kuan Yew Cheong, Khairunisak Abdul Razak, Fig. 1c), **c** 0.15, and **d** 0.2 and the corresponding particle size distribution **e** 0.05 and **f** 0.15

When the concentration of precursor was low ($[Sb^{3+}]/[N_2H_5OH] = 0.05$), well-distributed Sb_2O_3 nanoaparticles with spherical shape (Fig. 8a) and mean particle size of 5.01 nm (Fig. 8e) were observed. However, relatively lesser particles were formed, as shown in Fig. 8a. The low yield phenomenon can be due to insufficient supply of precursor during initial stage of synthesizing the Sb_2O_3 nanoparticles. In this study, precursor was a main chemical substance that will supply ion Sb for synthesizing Sb_2O_3 nanoparticles. As concentration of precursor increased to 0.1 and 0.15, particle size was gradually increased as shown in Fig. 9. This trend had been reported by other researchers [21, 24]. However, the low yield phenomenon had been improved, where more well-distributed nanoparticles (2–12 nm) with spherical shape were formed, as presented in Fig. 8b and c. Relative to other reported findings [2, 11, 13, 17], this method was able to synthesize spherical shape of Sb_2O_3 nanoparticles with a smaller mean particle size (4.72 nm) and a narrower particle size distribution (2–12 nm). Besides, particle size distribution also became broader, from 2–12 nm to 4–20 nm (mean particle size: 12.25 nm) (Fig. 8f) as concentration of precursor increased from 0.1 to 0.15. Larger particles were found in 0.15 concentration of precursor and the increment in particle size may be due to ripening effect [26], where smaller particles with higher surface energy favored to dissolve into larger particles. Nevertheless, fibrous materials formed when concentration of precursor increased to 0.2, as shown in Fig. 8d. This may be due to insufficient supply of hydrazine, which acted as a reduction agent to reduce ion Sb^{3+} to Sb atom completely when concentration of precursor was increased.

XRD patterns of Sb_2O_3 nanoparticles prepared with different concentrations of precursor are shown in Fig. 10. A total of 13 diffraction peaks were perfectly indexed to cubic phase of Sb_2O_3 (ICDD file no. 00-043-1071). Those diffraction peaks were associated with (222), (400), (331), (440), (622), (444), (551), (731), (800), (733), (662), (840) and (844) planes, as shown in Fig. 10. It was revealed that no other impurities were detected, apart from pure cubic

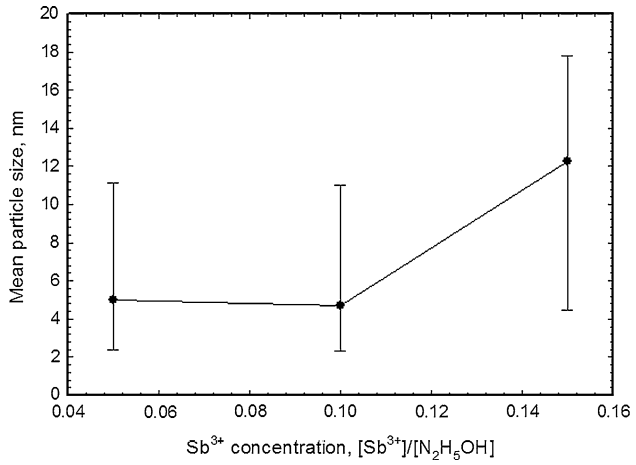

Fig. 9 Effect of concentration of precursor on particle size of Sb_2O_3 nanoparticles. The *error bars* indicate the maximum, minimum, and mean values of the particle size. (Particle size at $[Sb^{3+}]/[N_2H_5OH] = 0.2$ could not measure because no particles were observed)

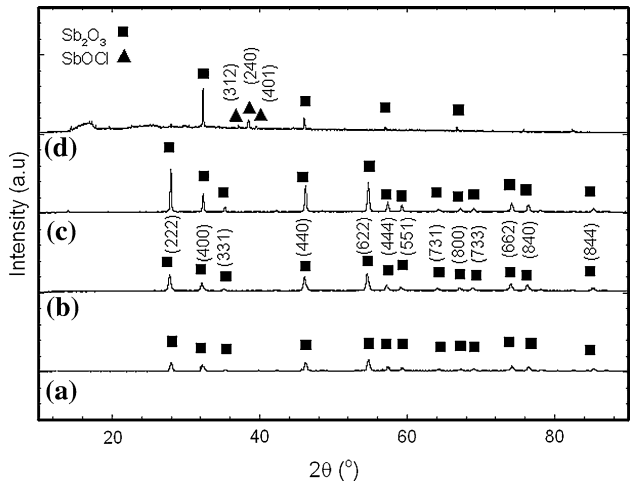

Fig. 10 XRD patterns of Sb_2O_3 nanoparticles with effect of concentration of precursor $[Sb^{3+}]/[N_2H_5OH] = (a)$ 0.05, (b) 0.1 [28], (c) 0.15 and (d) 0.2

phase of Sb_2O_3. In addition, Zhang et al. [11] and Zeng et al. [16] also reported similar findings. As concentration of precursor increased from 0.05 to 0.15, the diffraction peaks became stronger and higher intensity (Fig. 10a–c), which was related to the increase in particle size of Sb_2O_3 nanoparticles, as shown in Fig. 9. By further increasing the concentration of precursor to 0.2, mixture of amorphous and polycrystalline phases was detected as presented in Fig. 10d. The amorphous phase occurred at $2\theta < 27°$, while two types of polycrystalline phases were detected. The polycrystalline phases consisted of four diffraction peaks [(400), (440), (444) and (800) planes] of Sb_2O_3 and three diffraction peaks [(312), (240) and (401) planes] of SbOCl (ICDD file no. 01-073-2196).

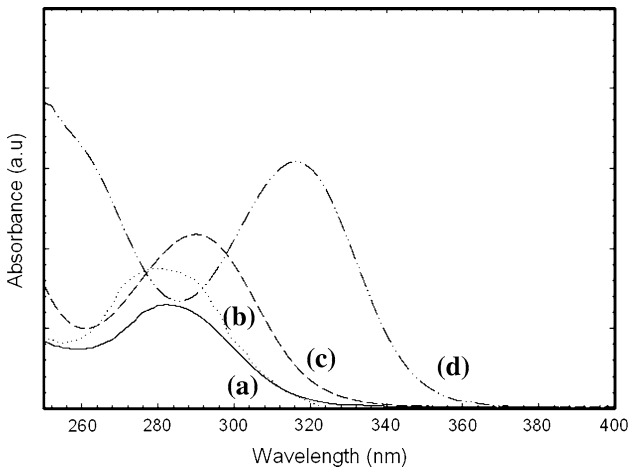

Fig. 11 UV–vis absorption spectra of Sb_2O_3 nanoparticles with effect of concentrations of precursor $[Sb^{3+}]/[N_2H_5OH] = (a)$ 0.05, (b) 0.1 [28], (c) 0.15, and (d) 0.2

Figure 11 presents UV–vis absorption spectra of Sb_2O_3 nanoparticles with effect of concentration of precursor ($[Sb^{3+}]/[N_2H_5OH] = 0.05$, 0.15, and 0.2). From the UV–vis absorption spectra, the maximum absorption wavelengths ranged from 280 to 316 nm, which are well consistent with the findings from other researchers, in which the reported maximum absorption wavelengths are occurred from 200 to 360 nm [15] and 250 to 300 nm [30]. Lowest absorbance intensity was revealed at the lowest concentration of precursor ($[Sb^{3+}]/[N_2H_5OH] = 0.05$). This matched with the TEM morphology (lower yield of particle), as shown in Fig. 10a. The maximum absorption wavelength of this concentration occurred at 282 nm. When concentration of precursor increased to 0.1, the maximum absorption wavelength appeared at 280 nm with higher absorbance intensity as compared to concentration of precursor at 0.05. This occurrence was due to the consequence from the yield improvement of particle. The maximum absorption wavelength was shifted to the higher wavelength at 290 nm, when concentration of precursor increased to 0.15. The shifting effect [26] indicated that the particle size became larger (mean particle size: 12.25 nm) as compared to concentration of precursor at 0.1 (mean particle size: 4.72 nm). This observation is also reflected in TEM images, as shown in Fig. 10b and c. Furthermore, fibrous materials (Fig. 10d) formed at a higher concentration of precursor ($[Sb^{3+}]/[N_2H_5OH] = 0.2$) and a longer maximum absorption wavelength was revealed at 316 nm as compared to other maximum absorption wavelengths.

Effect of boiling temperature

To understand the effect of boiling temperature on the particle size, shape, and size distribution of the

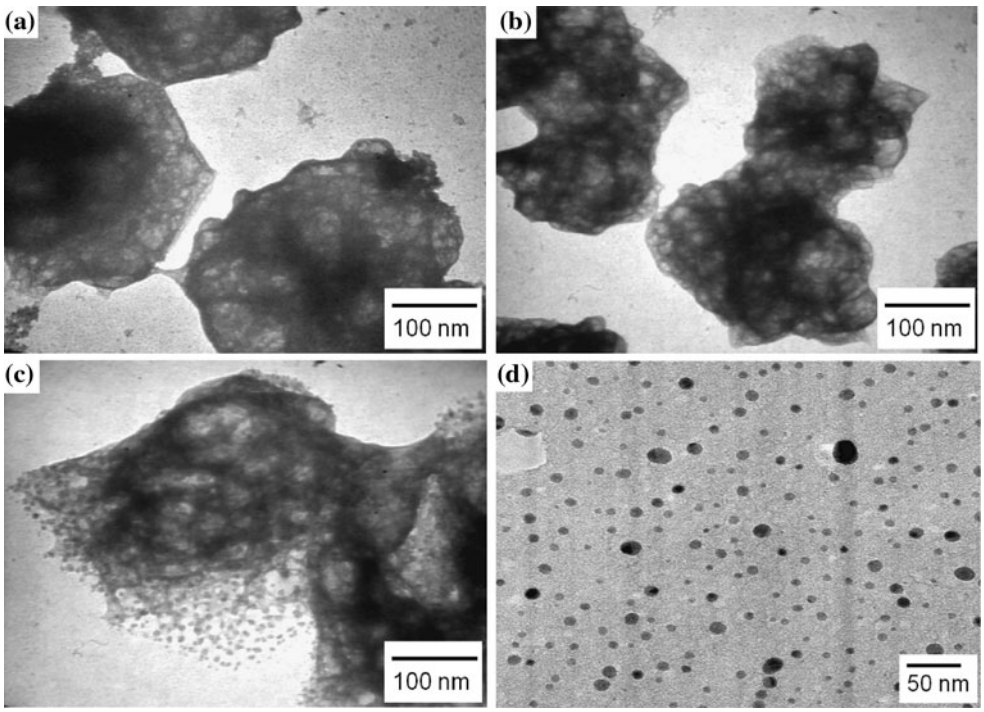

Fig. 12 TEM images of Sb_2O_3 nanoparticles with effect of boiling temperature **a** 25 °C, **b** 50 °C, **c** 80 °C, and **d** 110 °C [28] (With kind permission from Springer Science+Business Media: Journal of Nanoparticle Research, Controlled synthesis of Sb_2O_3 nanoparticles by chemical reducing method in ethylene glycol, DOI 10.1007/s11051-010-0169-y, 2010, Hui Shun Chin, Kuan Yew Cheong, Khairunisak Abdul Razak, Fig. 1c)

nanoparticles, other process parameters are kept invariable. Those process parameters were concentration of hydrazine at $[N_2H_5OH]/[Sb^{3+}] = 10$, concentration of NaOH at $[NaOH]/[Sb^{3+}] = 3$, reaction temperature at 120 °C, reaction time at 60 min, and concentration of precursor at $[Sb^{3+}]/[N_2H_5OH] = 0.1$.

Transmission electron microscope (TEM) images and particle size of Sb_2O_3 nanoparticles with effect of boiling temperature are presented in Fig. 12. The investigated boiling temperatures were 25, 50, 80, and 110 °C. Figure 12a and b shows fibrous materials were formed when boiling temperature was altered between 25 and 50 °C. The fibrous materials are believed to be some complex compound formed from $SbCl_3$, NaOH, hydrazine, and EG. No nanoparticles were formed in this range of temperature as hydrazine was added to the un-boiled mixture. This observation may be associated to the lack of spontaneous reaction between hydrazine and the mixture ($SbCl_3$ and NaOH in EG). Spontaneous reaction may occur if hydrazine was added to the boiled mixture. Literature [25] showed that spontaneous reaction is needed to gain an optimum reduction. When the boiling temperature of mixture was increased to 80 °C (the mixture was not boiled), combination of fibrous materials and nanoparticles were formed, as shown in Fig. 12c. When hydrazine was added to the boiled mixture (110 °C), well-dispersed Sb_2O_3 nanoparticles with spherical shape were synthesized, as shown in Fig. 12d. Thus, it was proven that hydrazine performed well when it was added to the boiled mixture. The mean particle size of Sb_2O_3 nanoparticles synthesized at 110 °C (boiling temperature) was 4.72 nm, while no data was available for 25, 50, and 80 °C, as no nanoparticles were formed. Literature reported that Sb_2O_3 nanoparticles had been synthesized in polyhedral shape with less than 200 nm via chemical method [11]. Thus, this chemical reduction method is able to overcome the limitation, in which well-distributed (2–12 nm), smaller (4.72 nm), and spherical shape of Sb_2O_3 nanoparticles were synthesized.

Figure 13 shows XRD patterns of Sb_2O_3 nanoparticles prepared at different boiling temperatures. At 25 °C, two diffraction peaks of $SbCl_3$ were detected, which are associated with (111) and (021) planes. Apart from that, a total of 14 diffraction peaks could be indexed to cubic phase of Sb_2O_3 (ICDD file no. 00-043-1071), which are associated with (111), (222), (400), (331), (440), (622), (444), (551), (731), (800), (733), (662), (840) and (844) planes, as shown in Fig. 13a. When hydrazine was added to the mixture with temperature of 50 °C, the two diffraction peaks of $SbCl_3$ [(111) and (021) planes] gradually decreased, while one of the diffraction peaks of Sb_2O_3 [(111) plane] increased, as shown in Fig. 13b. The diffraction peaks of $SbCl_3$ were due to the incomplete reduction of ion Sb^{3+}, since no spontaneous reaction took part. On the other hand, diffraction

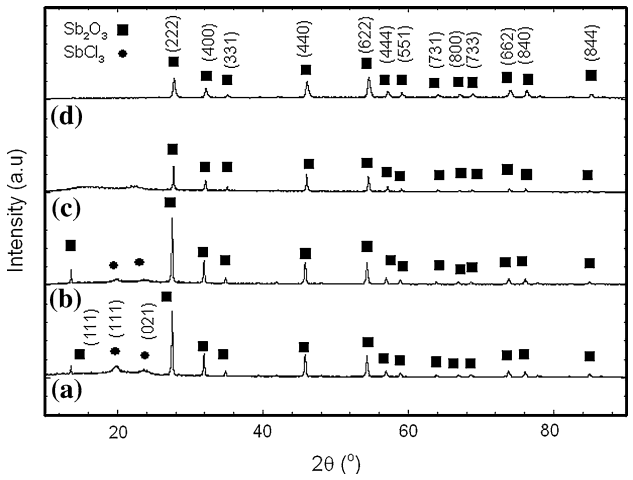

Fig. 13 XRD patterns of Sb_2O_3 nanoparticles with effect of boiling temperature (*a*) 25 °C, (*b*) 50 °C, (*c*) 80 °C and (*d*) 110 °C [28]

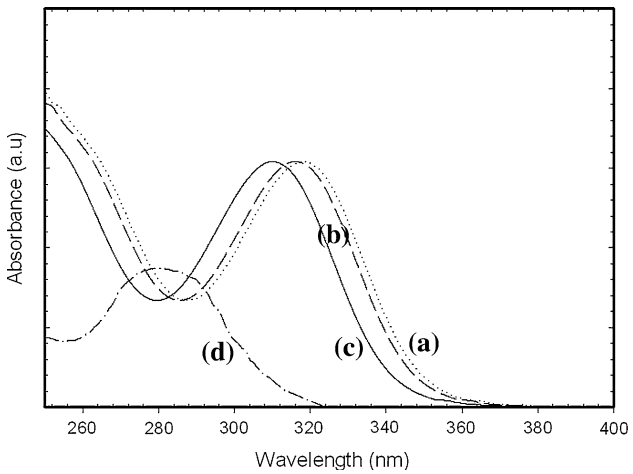

Fig. 14 UV–vis absorption spectra of Sb_2O_3 nanoparticles with effect of boiling temperature (*a*) 25 °C, (*b*) 50 °C, (*c*) 80 °C, and (*d*) 110 °C [28]

peaks of Sb_2O_3 were due to the subsequent heating at 120 °C for 60 min, in which partial Sb_2O_3 phases were promoted. Mixture of amorphous and polycrystalline phases was detected at 80 °C. The amorphous phase was detected at diffraction angle <27°, while a total of 13 diffraction peaks matched with cubic phase of Sb_2O_3 (ICDD file no. 00-043-1071), as shown in Fig. 13c. The 13 diffraction peaks are associated with (222), (400), (331), (440), (622), (444), (551), (731), (800), (733), (662), (840), and (844) planes. Moreover, the two diffraction peaks of $SbCl_3$ were disappeared at 80 °C. Figure 13d shows diffraction peak of Sb_2O_3 nanoparticles prepared at 110 °C. Similar diffraction peaks were detected as compared to temperature at 80 °C. Those diffraction peaks exhibited good crystallinity (no amorphous phase) and high purity (no impurities). Similar findings had been reported by Zhang et al. [11] and Zeng et al. [16].

UV–vis absorption spectra of Sb_2O_3 nanoparticles with effect of boiling temperature (25, 50, 80, and 110 °C) are presented in Fig. 14. From the UV–vis absorption spectra, the sequenced (from higher to lower) maximum absorption wavelengths were 318, 316, 310, and 280 nm, with respective to the boiling temperatures at 25, 50, 80, and 110 °C (mean particle size: 4.72 nm). The detected maximum absorption wavelengths are comparable with the earlier reported finding, where the maximum absorption wavelengths of Sb_2O_3 ranged from 200 to 360 nm [15] and 250 to 300 nm [30]. The shifting of maximum absorption wavelength to a higher wavelength was mainly due to the various particle sizes and formation of fibrous materials [26]. In the case of absorbance intensity, there was a similarity of intensity with temperatures at 25, 50, and 80 °C. However, lower absorbance intensity was revealed at temperature 110 °C. The difference in the absorbance intensity was due to the formation of fibrous materials, as shown in Fig. 12a–c.

Conclusions

In summary, a detailed investigation of the chemical reduction method approach to synthesize Sb_2O_3 nanoparticles was carried out. Well-distributed and spherical shape of Sb_2O_3 nanoparticles with particle size ranges of 2–12 nm have been successfully synthesized by reducing $SbCl_3$ with hydrazine in EG. Effects of reaction temperature, reaction time, precursor concentration and boiling temperature on the particle size, shape, and distribution of the Sb_2O_3 have been discussed. XRD revealed that the nanoparticles were indexed as the cubic phase of Sb_2O_3. The UV–vis maximum absorption wavelengths of Sb_2O_3 nanoparticles occurred in the range of 280–318 nm. Relationship between UV–vis absorption wavelength of the nanoparticles and their particle size of aforementioned effects were explored. The particle size and UV–vis absorption wavelength increased when reaction temperature, reaction time, and concentrations of $SbCl_3$ were increased. Therefore, aiming to synthesize well-distributed and smaller nanoaparticles with spherical shape, the proposed process parameters are: reaction temperature at 120 °C, reaction time at 60 min, concentration of precursor ($[Sb^{3+}]$/$[N_2H_5OH]$) at 0.1, and boiling temperature at 110 °C.

Acknowledgements One of the authors (H.S.C) would like to thank USM RU-PRGS grant and USM fellowship for the scholarship and financial support on this project. Another author (K.Y.C) would like to acknowledge the financial support given by Short Term Grant of Universiti Sains Malaysia (6039038).

References

1. Wang D, Zhou Y, Song C, Shao M (2009) J Cryst Growth 311:3948

2. Ye CH, Wang GY, Kong MG, Zhang LD (2006) J Nanomater 2006:1
3. Xie XL, Li RKY, Liu QX, Mai YW (2004) Polymer 45:2793
4. Feng L, Wang J, Liu J, Wang B, Song S (2007) J Compos Mater 41:1487
5. Laachachi A, Cochez M, Ferriol M, Leroy E, Lopez Cuesta JM, Oget N (2004) Polym Degrad Stab 85:641
6. Duh B (2002) Polymer 43:3147
7. Nalin M, Messaddeq Y, Ribeiro SJL, Poulain M, Briois V (2001) J Optoelectron Adv Mater 3:553
8. Sahoo NK, Apparao KVSR (1997) Appl Phys A 63:195
9. Ozawa K, Sakka Y, Amano M (1998) J Mater Res 13:830
10. Dzimitrowicz DJ, Goodenough JB, Wiseman PJ (1982) Mater Res Bull 17:971
11. Zhang ZL, Guo L, Wang WD (2001) J Mater Res 16:803
12. Jha AK, Prasad K (2009) Biochem Eng J 43:303
13. Chen XY, Huh HS, Lee SW (2008) J Solid State Chem 181:2127
14. Liu YP, Zhang YH, Zhang MW, Zhang WH, Qian YT, Yang L, Wang CS, Chen ZW (1997) Mater Sci Eng B 49:42
15. Zeng DW, Zhu BL, Xie CS, Song WL, Wang AH (2004) Mater Sci Eng A 366:332
16. Zeng DW, Xie CS, Zhu BL, Song WL (2004) Mater Lett 58:312
17. Xu CH, Shi SQ, Surya C, Woo CH (2007) J Mater Sci 42:9855. doi:10.1007/s10853-007-1799-z
18. Qiu KQ, Zhang RL (2006) Vacuum 80:1016
19. Chin HS, Cheong KY, Abdul Razak K (2010) J Mater Sci 45:5993. doi:10.1007/s10853-010-4849-x
20. Wu SH, Chen DH (2003) J Colloid Interface Sci 259:282
21. Balela MDL (2008) Dissertation, Universiti Sains Malaysia, Penang
22. Lee YM, Qin GW, Lee CG, Koo BH, Moon KY, Shimada Y, Kitakami O (2007) Met Mater Int 13:207
23. Kim KD, Kim HT (2003) Mater Lett 2003:3211
24. Pattabi M, Saraswathi AB (2007) J New Mater Electrochem Syst 10:43
25. Yang M, Zhang Y, Pang G, Feng S (2007) Eur J Inorg Chem 2007:3841
26. Segets D, Tomalino LM, Gradl J, Peukert W (2009) J Phys Chem C 113:11995
27. Zhang G, Roy BK, Allard LF, Cho J (2008) J Am Ceram Soc 91:3875
28. Chin HS, Cheong KY, Abdul Razak K (2010) J Nanoparticle Res. doi:10.1007/s11051-010-0169-y
29. Rautio J, Perämäki P, Honkamo J, Jantunen H (2009) Microchem J 91:272
30. Chang PR, Yu J, Ma X (2009) Macromol Mater Eng 294:762